Journal of Advanced Ceramics
2018, **7**(1): 79–87
https://doi.org/10.1007/s40145-018-0259-3
ISSN 2226-4108
CN 10-1154/TQ

Research Article

Multi-phase structure and electrical properties of $Bi_{0.5}Li_{0.5}ZrO_3$ doping $K_{0.48}Na_{0.56}NbO_3$ lead-free piezoelectric ceramics

Xiaoyan PENG[a,b], Boping ZHANG[a,*], Lifeng ZHU[a], Lei ZHAO[c], Ruixiao MA[a], Bo LIU[a], Xiaodong WANG[a]

[a]*School of Materials Science and Engineering, University of Science and Technology Beijing, Beijing 100083, China*
[b]*New Metallurgy Hi-Tech Group Co., Ltd., China Iron & Steel Research Institute Group, Beijing 100081, China*
[c]*Hebei Key Lab of Optic-Electronic Information and Materials, College of Physics Science & Technology, Hebei University, Baoding 071002, China*

Received: November 07, 2017; Revised: January 13, 2018; Accepted: January 14, 2018

Abstract: $(1–x)K_{0.48}Na_{0.56}NbO_3–xBi_{0.5}Li_{0.5}ZrO_3$ (KNN–*x*BLZ, x = 0–0.06) lead-free piezoelectric ceramics were prepared by the conventional solid-state sintering method, and their phase structures and electric properties as well as T_C were systematically investigated. The orthorhombic–tetragonal (O–T) two phases were detected in all $(1–x)K_{0.48}Na_{0.56}NbO_3–xBi_{0.5}Li_{0.5}ZrO_3$ ceramics at $0.01 \leqslant x \leqslant 0.05$. Due to the appropriate ratio between O phase and T phase (C_O / C_T = 45/55), high piezoelectric properties of d_{33} = 239 pC/N, k_p = 34%, and P_r = 25.23 μC/cm^2 were obtained at x = 0.04. Moreover, a high T_C = 348 ℃ was also achieved in KNN–*x*BLZ ceramic at x = 0.04. These results indicate that $(1–x)K_{0.48}Na_{0.56}NbO_3–xBi_{0.5}Li_{0.5}ZrO_3$ system is a promising candidate for high-temperature piezoelectric devices.

Keywords: lead-free piezoelectric ceramics; potassium–sodium niobate (KNN); solid-state sintering; multi-phase; electrical properties

1 Introduction

Piezoelectric ceramics are widely used in sensors, transducers, actuators, and surface acoustic wave devices because of their ability to convert electrical energy into mechanical energy and vice versa [1]. Lead zirconate titanate (PZT) piezoelectric ceramics have been predominantly used in various applications due to their stronger piezoelectric effects so far. Unfortunately, the high lead content of 60% in the PZT ceramics is the environmentalist's nightmare as the lead toxicity severely threatens to human health and environment [2–4]. Thus, it is imminent to develop high-performance lead-free piezoelectric ceramics. In 2004, Saito *et al*. [5] created the textured potassium–sodium niobate (KNN) lead-free piezoceramics with the piezoelectric constant (d_{33}) of 416 pC/N which is close matched with those of PZT. In 2017, Zheng *et al.* [6] reported that the $0.965(K_{0.48}Na_{0.52})Nb_{0.95}Sb_{0.05}O_3–0.035Bi_{0.5}(K_{0.82}Na_{0.18})_{0.5}HfO_3$ ceramic had d_{33} = 525 pC/N. In addition, further high piezoelectric property of d_{33} = 570±10 pC/N has

* Corresponding author.
E-mail: bpzhang@ustb.edu.cn

been achieved in the $0.95(K_{1-w}Na_w)Nb_{0.965}Sb_{0.035}O_3$–$0.02BaZrO_3$–$0.03Bi_{0.5}K_{0.5}HfO_3$ composition [7]. Therefore, (K,Na)NbO_3 (KNN)-based lead-free ceramics have been considered as one of the most promising substitutes for lead-based piezoelectric ceramics [2–4,8].

It is well known that the pure KNN ceramics prepared by solid-state sintering exhibit a low piezoelectric constant d_{33} of only 80–125 pC/N [9–11]. Therefore, it is necessary to enhance the piezoelectric properties of KNN ceramics. Our previous work [12,13] indicated that excessive Na_2O which was to compensate the volatilization of Na^+ could effectively improve the piezoelectric properties by 10%–40% in KNN ceramics. Furthermore, d_{33} of KNN ceramics was increased by 188–324 pC/N as the replacement of K^+ and Na^+ with Li^+ in (K,Na,Li)NbO_3 system because of the appearance of polymorphic phase boundary (PPB) phase [14]. Thus, adding Li^+ to KNN ceramics can increase the Curie temperature (T_C), decrease the phase transition temperature of orthorhombic (O) and tetragonal (T) (T_{O-T}) to room temperature, slightly affect the phase transition temperature of rhombohedral (R) and O (T_{R-T}), decline the sintering temperature, and improve the density of KNN materials, besides improving the piezoelectric properties. To sum up, Li is a very popular and effective element in KNN system to enhance the piezoelectric properties and increase T_C. An enhanced d_{33} of KNN-based ceramics can also be attained by forming its solid solutions with ABO_3-type perovskite such as $LiNbO_3$, $LiTaO_3$, (Bi,Na,K,Li)ZrO_3, $Bi_{0.5}Li_{0.5}ZrO_3$, and so on.

Recently, the high piezoelectric property $d_{33} \approx$ 400 pC/N and electromechanical coupling factor (k_p) of 0.47 were achieved in $(1-x)K_{0.40}Na_{0.60}Nb_{0.965}Sb_{0.035}O_3$–$xBi_{0.5}Li_{0.5}ZrO_3$ (KNNS–BLZ) system because of the coexistence of R and T phases near the morphotropic phase boundary (MPB) at x = 0.03, as reported by Zheng *et al.* [15]. The piezoelectric properties of KNNS–BLZ ceramics prepared by solid-state sintering show a significant breakthrough, compared with the PZT system; however, its T_C (only 292 ℃) for KNNS–0.03BLZ ceramic needs to be improved to fit for the demand of practical application. The reports about Bi^{3+} (or Ba^{2+}), Li^+, and Zr^{4+} doping KNN lead-free piezoelectric ceramics are illustrated in Table 1 [15–27]. Li *et al.* [4] indicated that the T_C of KNN system decreased as introducing of Sb^{5+} ion. As shown in Table 1, T_C of Sb doping KNN-based piezoelectric ceramics is only 175–292 ℃; moreover, Sb^{5+} is toxic. Since alkali K and Na ions are easy to volatilize when the sintering temperature is above 1000 ℃, adding excessive alkali Na could be in favor of reducing the sintering temperature of KNN-based ceramics, replenishing the decreased amount of alkali Na and K volatilized [13,28,29] and improving the piezoelectric properties. Zhang *et al.* [10] reported that high density

Table 1 Phase structure and electrical properties of Bi^{3+} (or Ba^{2+}), Li^+, and Zr^{4+} doped KNN lead-free piezoelectric ceramics

Ceramic system	Phase structure	d_{33} (pC/N)	T_C (℃)	k_p (%)	E_c (kV/cm)	P_r (μC/cm^2)	Ref.
$0.96(K_{0.48}Na_{0.56})(Nb_{0.95}Sb_{0.05})O_3$–$0.04(Bi_{0.8}La_{0.2})_{0.5}(Na_{0.8}Li_{0.2})_{0.5}ZrO_3$	R–T	470	210	50	7.1	16.5	Jiang *et al.* [16]
$0.975(K_{0.40}Na_{0.60})_{0.985}Li_{0.015}(Nb_{0.94}Sb_{0.06})O_3$–$0.025Bi_{0.5}Na_{0.5}ZrO_3$	R–T	390	250	—	—	—	Yuan *et al.* [17]
$0.92(Na_{0.5}K_{0.5})NbO_3$–$0.06BaZrO_3$–$0.02(Bi_{0.5}Li_{0.5})TiO_3$	PC–T	321	256	53	—	—	Shi *et al.* [18]
$0.96(K_{0.48}Na_{0.52})(Nb_{0.95}Sb_{0.05})O_3$–$0.04(Bi_{0.5}Li_{0.5})ZrO_3$	R–T	330	230	—	—	14.5	Zheng *et al.* [19]
$0.92(Na_{0.5}K_{0.5})NbO_3$–$0.02(Bi_{1/2}Li_{1/2})TiO_3$–$0.06BaZrO_3$	R–T	348	243	57	—	—	Wang *et al.* [20]
$0.955K_{0.48}Na_{0.52}NbO_3$–$0.01Bi_{0.5}Na_{0.5}TiO_3$–$0.035Bi_{0.5}(Na_{0.7}K_{0.2}Li_{0.1})_{0.5}ZrO_3$	R–T	310	338	45	17.4	23.4	Cheng *et al.* [21]
$0.955K_{0.48}Na_{0.52}NbO_3$–$0.005BiScO_3$–$0.04Bi_{0.5}(Na_{0.7}K_{0.2}Li_{0.1})_{0.5}ZrO_3$	R–T	366	335	47	—	—	Cheng *et al.* [22]
$0.97K_{0.40}Na_{0.60}Nb_{0.965}Sb_{0.035}O_3$–$0.03Bi_{0.5}Li_{0.5}ZrO_3$	R–T	400	292	47	—	—	Zheng *et al.* [15]
$0.95(K_{0.50}Na_{0.50})_{0.97}Li_{0.03}Nb_{0.97}Sb_{0.03}O_3$–$0.05BaZrO_3$	R–O	235	267	44	—	21.0	Zhang *et al.* [23]
$0.90(Na_{0.5}K_{0.5})NbO_3$–$0.07BaZrO_3$–$0.03(Bi_{0.5}Li_{0.5})TiO_3$	R–T	263	206	40.6	—	—	Zushi *et al.* [24]
$0.96(K_{0.48}Na_{0.52})(Nb_{0.95}Sb_{0.05})O_3$–$0.04Bi_{0.5}(Na_{0.7}K_{0.2}Li_{0.1})_{0.5}ZrO_3$	R–T	380	290	46	—	—	Cheng *et al.* [25]
$0.96(K_{0.5}Na_{0.5})_{0.95}Li_{0.05}Nb_{0.93}Sb_{0.07}O_3$–$0.04BaZrO_3$	R–T	425	197	50	—	15.8	Zhang *et al.* [26]
$0.94(K_{0.34}Na_{0.6}Ba_{0.06}Nb_{0.94}Zr_{0.06})O_3$–$0.06LiSbO_3$	R–O–T	344	175	32	—	—	Liang *et al.* [27]
$0.96K_{0.48}Na_{0.56}NbO_3$–$0.04Bi_{0.5}Li_{0.5}ZrO_3$	O–T	239	348	34	15.2	25.2	This work

(relative density over 95%) and piezoelectric constant d_{33} = 279 pC/N were achieved by adding excessive Na in the $Li_{0.058}(Na_{0.52+x}K_{0.48})_{0.942}NbO_3$ ceramic as x = 0.015 sintering at a lower temperature 1000 ℃. Thus, in the present investigation, the $(1–x)K_{0.48}Na_{0.56}NbO_3–xBi_{0.5}Li_{0.5}ZrO_3$ (KNN–xBLZ, x = 0–0.06) system with excessive Na^+ content was designed to obtain both high T_C and piezoelectric properties. The phase structures, electric properties, and T_C of KNN–xBLZ ceramics were systematically investigated. The O–T two phases were detected in KNN–xBLZ ceramics at $0.01 \leqslant x \leqslant 0.05$ and the proportions of O to T phase were carefully calculated by Gaussian–Lorentzian curve-fitting method. Because of the appropriate ratio of O and T phases, high piezoelectric property d_{33} = 239 pC/N, electromechanical coupling factor k_p = 34%, and remanent polarization P_r = 25.23 μC/cm^2 were achieved at x = 0.04. Moreover, a high T_C = 348 ℃ was also achieved in KNN–xBLZ ceramic at x = 0.04, which indicated that the KNN–xBLZ system had promising prospects in high-temperature piezoelectric devices.

2 Experimental

$(1–x)K_{0.48}Na_{0.56}NbO_3–xBi_{0.5}Li_{0.5}ZrO_3$ (x = 0–0.06) ceramics were prepared by the conventional solid sintering method. Potassium carbonate (K_2CO_3, 99%), lithium carbonate (Li_2CO_3, 99.5%), sodium carbonate (Na_2CO_3, 99.8%), niobium oxide (Nb_2O_5, 99.95%), zirconium dioxide (ZrO_2, 99%), and bismuth oxide (Bi_2O_3, 99%) were used as raw materials. These powders were weighed according to the chemical formula, and ball mixed with ethanol solution in a planetary ball mill. After ball milling for 4 h, the slurry was dried and then calcined at 750 ℃ for 4 h. The synthesized powders were subsequently compacted into a disk of 10.0 mm in diameter and 1.0 mm in thickness with pressure of 80 MPa using PVA as a binder. The pellets were sintered in air at 1110 ℃ for 3 h. Silver paste was covered on both surfaces of the samples as electrodes and then the samples were polarized under a DC field of 3–4 kV/mm at 120 ℃ for 30 min in silicone oil bath for measuring the piezoelectric properties.

The microstructures were observed with scanning electron microscopy (FE-SEM; SUPRATM55, Carl Zeiss, Nakano, Japan). The densities of samples were tested by the Archimedes method. The crystal structures were determined by X-ray powder diffraction with a Cu Kα radiation (λ = 0.15416 nm) filtered through a Ni foil (Rigaku; RAD-B system, Tokyo, Japan). The coexistence of O–T phases was identified by Gaussian–Lorentzian curve-fitting method. The percentages of O phase and T phase were acquired by calculating the area of resolved peaks. The lattice parameters were calculated from the angle of resolved peaks.

The temperature dependence of dielectric properties was examined by using a programmable furnace with an LCR analyzer (TH2828S, Tonghui Electronics, China) in the temperature range of 20–500 ℃. The piezoelectric constant d_{33} was measured with a quasistatic piezoelectric constant testing meter (ZJ-3A, Institute of Acoustics, Chinese Academy of Sciences). Ferroelectric hysteresis loop was measured at room temperature by using a ferroelectric tester (RT6000HVA, Radiant).

3 Results and discussion

3.1 Microstructure

Figure 1 shows the SEM images of the fracture surfaces and densities for KNN–xBLZ ceramics sintered at 1110 ℃ for 3 h. An obvious liquid phase with a vague grain boundary is observed when x = 0 in Fig. 1(a). The relative density of the ceramic is 83%, as shown in Fig. 1(g). The appearance of liquid phase may be because of the high sintering temperature and the excessive Na_2O. The phase graph reported by Jaffe *et al.* [1] showed that the liquid would appear at 1110 ℃ in the $K_{0.48}Na_{0.52}NbO_3$ ceramic and the excessive Na_2O would supply more liquid phase. Therefore, the liquid phase cannot diffuse into matrix completely at high temperature, and consequently becomes condensate in the grain boundary. More liquid phase is detected at x = 0.01 in Fig. 1(b) along with an enhanced relative density up to 89%, which is attributed to the formation of a low co-melting point compound corresponding to $Li_2O–K_2O–Na_2O$ [30] due to adding BLZ in KNN–xBLZ ceramics. When $x \geqslant 0.02$ (Fig. 1(c)), besides clear grain boundaries, a small number of pores around grain boundaries are observed. This is owing to the raised sintering temperature of densification by introducing of Zr^{4+}. The increased Zr^{4+} causes the rise of sintering temperature and consequently the sintering becomes difficult, which leads to decreased grain size. The grain

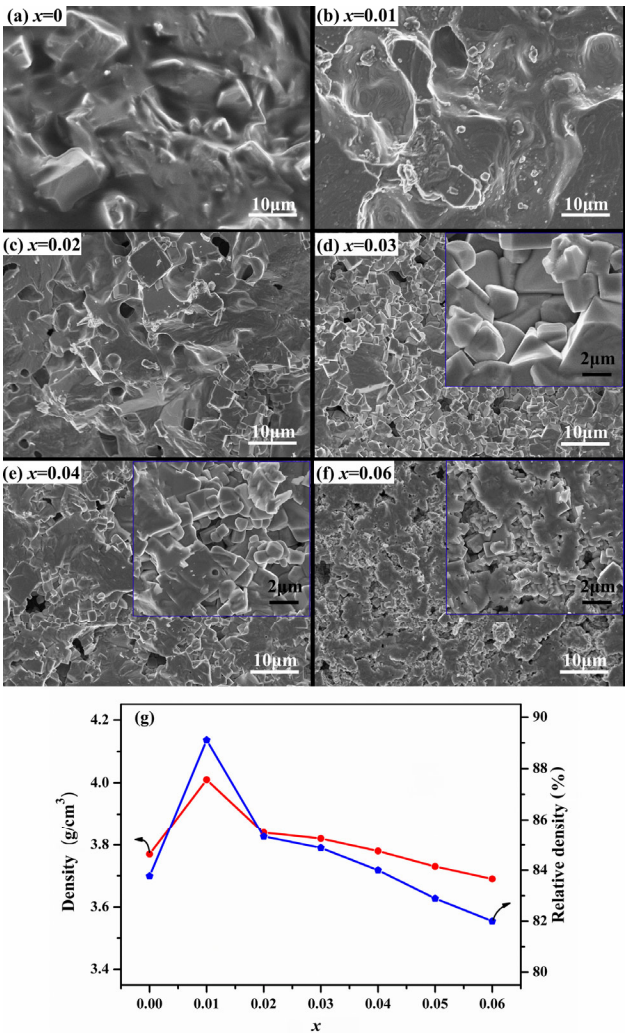

Fig. 1 Microstructure of KNN–*x*BLZ ceramics: (a) $x = 0$, (b) $x = 0.01$, (c) $x = 0.02$, (d) $x = 0.03$, (e) $x = 0.04$, (f) $x = 0.06$; and (g) density and relative density.

size is about 2 μm when $x = 0.03$ in Fig. 1(d), except for few 5–6 μm big particles, and decreases to 1 μm at $x = 0.04$ in Fig. 1(e). The refined grain size with more uniform distribution is produced with the increase of x to 0.06. The high density of 4.01 g/cm^3 and relative density of 89.11% of KNN–*x*BLZ ceramic are achieved at $x = 0.01$, which is owing to the appearance of liquid phase as shown in Fig. 1(b). Due to the increase of the sintering temperature of densification as introducing of Zr^{4+}, the relative density of ceramics decreases when $x \geqslant 0.02$, which is consistent with SEM images as shown in Figs. 1(a)–1(f).

3. 2 Phase structure

Figure 2 shows the XRD patterns of KNN–*x*BLZ ceramics sintered at 1110 ℃ for 3 h. All samples exhibit a pure perovskite structure without any trace of impurity phase, which indicates that BLZ has diffused into KNN lattices to form a homogeneous solid solution. The standard diffraction peaks cited from $KNbO_3$ with orthorhombic (O) symmetry (PDF#71-0946) and tetragonal (T) symmetry (PDF#71-0945) are presented by vertical lines for comparison. The difference between O and T phases is usually focused on the diffraction intensity ratio around 45°. $I_{O(022)} / I_{O(200)}$ ratio is larger than 2:1, while $I_{T(002)} / I_{T(200)}$ ratio turns to smaller than 1:2. Figure 3 shows the *x*-evolved diffraction peaks around 45°. The simulated 2θ and intensity by Gaussian–Lorentzian curve-fitting method are listed in Table 2.

When $x = 0$, the diffraction peaks in Fig. 3(a) correspond to O phase characteristic, whose $I_{O(022)} / I_{O(200)}$ ratio is larger than 2:1. After adding BLZ, $I_{O(022)} / I_{O(200)}$ ratio is lower than 2:1, which indicates the appearance of T phase.

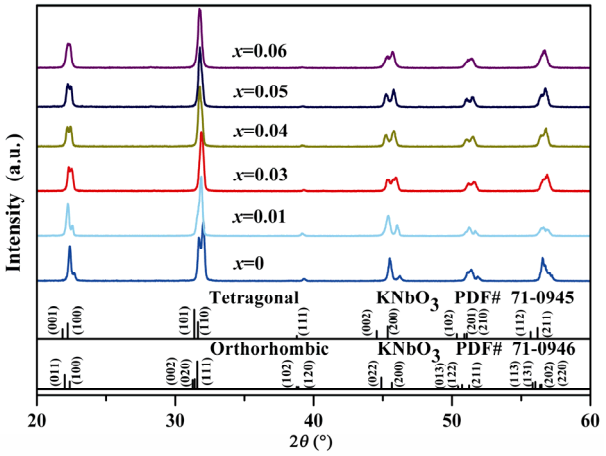

Fig. 2 XRD patterns for KNN–*x*BLZ ceramics sintered at 1110 ℃.

Table 2 2θ and intensity of fitting patterns of O and T phases

Sample	$O_{(022)}$		$O_{(200)}$		$T_{(002)}$		$T_{(200)}$	
	2θ (°)	I	2θ (°)	I	2θ (°)	I	2θ (°)	I
O (PDF#71-0946)	44.90	36.10	45.65	17.40	—	—	—	—
T (PDF#71-0945)	—	—	—	—	44.56	18.10	45.35	34.70
$x = 0$	45.51	5933	46.21	1237	—	—	—	—
$x = 0.01$	45.38	8329	46.04	3943	45.24	551	45.94	971
$x = 0.03$	45.42	2645	45.91	1343	45.28	1509	45.86	3219
$x = 0.04$	45.37	2041	45.89	1214	45.21	2775	45.78	4722
$x = 0.05$	45.37	1330	45.87	813	45.22	2312	45.78	3714
$x = 0.06$	45.36	506	45.87	283	45.28	3010	45.71	4720

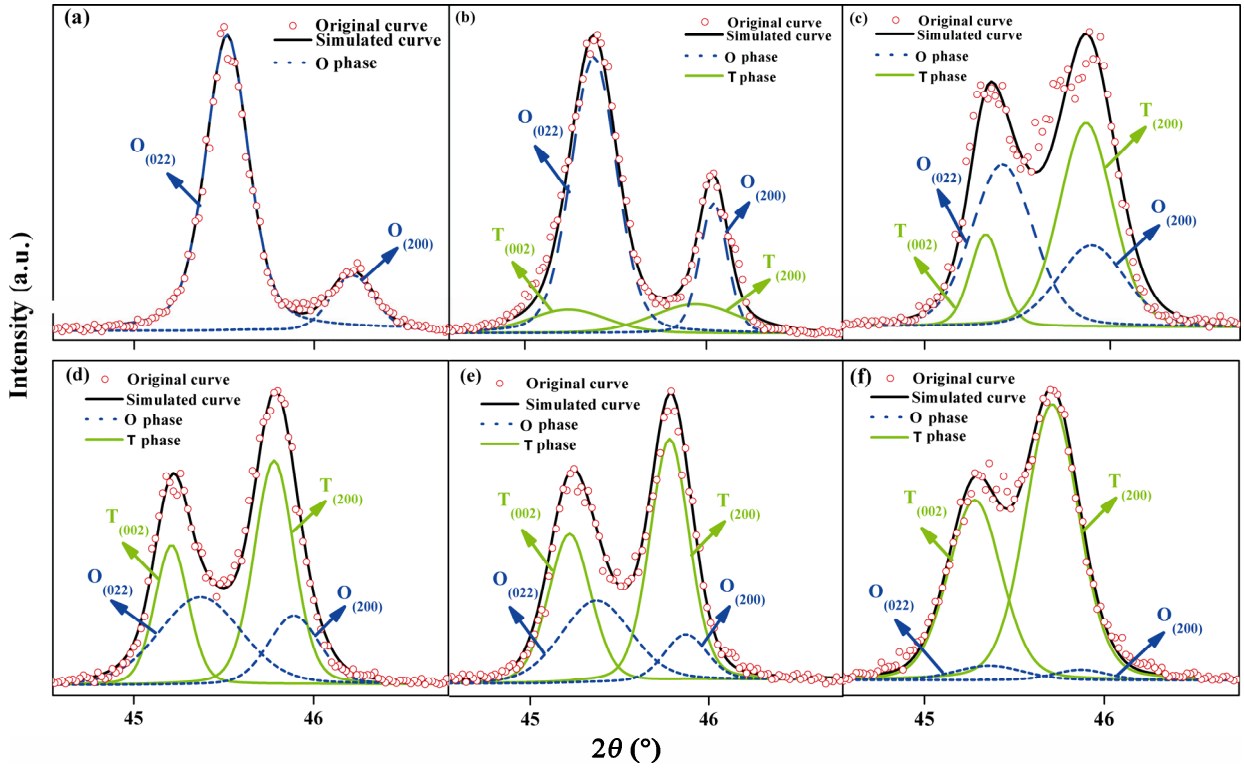

Fig. 3 Amplified XRD patterns simulated by Gaussian–Lorentzian curve-fitting method: (a) $x = 0$, (b) $x = 0.01$, (c) $x = 0.03$, (d) $x = 0.04$, (e) $x = 0.05$, (f) $x = 0.06$.

The simulated data confirm that phase structures of samples at $0.01 \leqslant x \leqslant 0.06$ are the coexisting O–T phases. According to Eq. (1), it can conclude that the O phase fraction decreases as x increasing. The more detailed variation for the O and T phase fraction is shown in Fig. 4(a). The main phase of samples is O symmetry when $x \leqslant 0.03$, while it turns to T phase when $x \geqslant 0.04$.

$$C_O / C_T = \frac{A_{O(022)} + A_{O(200)}}{A_{T(002)} + A_{T(200)}} \tag{1}$$

where C_O / C_T, $A_{O(022)}$, $A_{O(200)}$, $A_{T(002)}$, and $A_{T(200)}$ are the ratio of O and T phases, the integral area of $O_{(022)}$, $O_{(200)}$, $T_{(002)}$, and $T_{(200)}$ peaks. The lattice parameters a, b, and c for O and T phases calculated by Eqs. (2)–(4) are also shown in Figs. 4(b) and 4(c). a_O, b_O, and c_O exhibit a little changes as x increasing, suggesting that $Bi_{0.5}Li_{0.5}ZrO_3$ hardly enters into O phase lattice. a_T for T phase increases, while c_T and c_T/a_T decrease as x increasing. Here, the variation of lattice parameters means that the $Bi_{0.5}Li_{0.5}ZrO_3$ enters into T phase lattice.

$$2d \sin\theta = n\lambda \tag{2}$$

$$\frac{1}{d^2} = \frac{h^2}{a^2} + \frac{k^2}{b^2} + \frac{l^2}{c^2} \tag{3}$$

$$d = \frac{a}{\sqrt{h^2 + k^2 + l^2 \dfrac{a^2}{c^2}}} \tag{4}$$

where d and θ are crystalline interplanar spacing and diffraction angle respectively; a, b, and c are lattice parameters, as well as h, k, and l are crystal indices.

3.3 Electrical properties

Figure 5 shows the temperature dependence of dielectric constant ε_r (ε_r–T), dielectric loss factor $\tan\delta$ ($\tan\delta$–T) for KNN–xBLZ ceramics measured at 1 kHz between 20 and 450 ℃, as well as ε_r at room temperature and T_C, $T_{O\text{-}T}$ and T_C versus x for KNN–xBLZ ceramics. Two phase transition points corresponding to ferroelectric–ferroelectric phase transition $T_{O\text{-}T}$ and ferroelectric–paraelectric phase transition T_C are detected in all samples at the measured temperature range. $T_{O\text{-}T}$ and T_C are about 207 and 420 ℃ at $x = 0$ respectively and show the same linear declining trend as x increasing. As x increasing to 0.60, $T_{O\text{-}T}$ and T_C decrease to 57 and 291 ℃ as shown in Fig. 5(f), respectively. The detailed variation for $T_{O\text{-}T}$ and T_C versus x is shown in Fig. 5(g). The low $T_{O\text{-}T}$ further indicates that the O and T two phases should coexist at

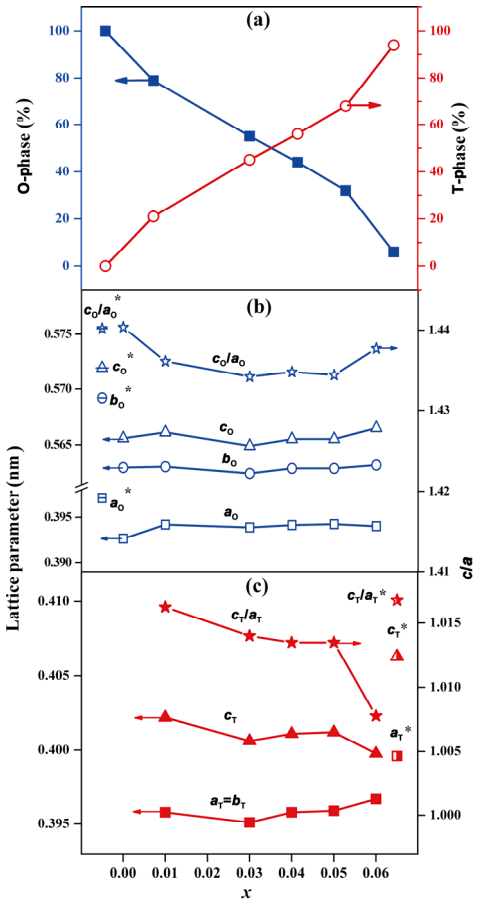

Fig. 4 Phase composition percent and lattice parameters calculated by simulating with Gaussian–Lorentzian curve-fitting method. Data from PDF index are marked with "*". (a) Area percent of O phase and T phase peak; (b) lattice parameters and *c*/*a* of O phase; (c) lattice parameters and *c*/*a* of T phase.

room temperature when $0.01 \leqslant x \leqslant 0.06$. As shown in Fig. 5(h), the dielectric constant at room temperature (ε_r at room temperature) of KNN–*x*BLZ ceramics increases with *x* except for $x = 0.05$, and the dielectric constants ε_r are 938 and 990 at $x = 0.04$ and 0.06, respectively. However, the dielectric constant at T_C (ε_r at T_C) of KNN–*x*BLZ ceramics shows a rise–fall trend and the highest ε_r reaches 6417 at $x = 0.03$.

Figure 6 shows the changes of d_{33}, k_p, and C_O / C_T as a function of *x* for the KNN–*x*BLZ ceramics. The d_{33} and k_p have the same rise–fall tendency. For the sample at $x = 0$, the d_{33} and k_p are 108 pC/N and 23.38%, respectively, and they reach the maximum values $d_{33} = 239$ pC/N and $k_p = 33.96\%$ as *x* increasing to 0.04. The C_O / C_T ratios of KNN–*x*BLZ ceramics are 100/0, 79/21, 55/45, 44/56, 32/68, and 4/96 when $x = 0$, 0.01, 0.03, 0.04, 0.05, and 0.06, respectively. It is well known that the phase structure plays a key role in enhancing the piezoelectric property [31–36]. Here, the high piezoelectric property of KNN–*x*BLZ ceramics is also attributed to the polycrystalline phase transition (PPT), which is O and T two-phase coexistence. Although the PPT lies in all KNN–*x*BLZ ceramics with $0.01 \leqslant x \leqslant 0.06$ as proved in Figs. 2, 3, and 5, the maximum values of d_{33} and k_p are only achieved at the composition of $x = 0.04$. This may be the result of decreasing C_O / C_T ratios with *x* increasing, as shown in Fig. 6. It can conclude that the maximum piezoelectric

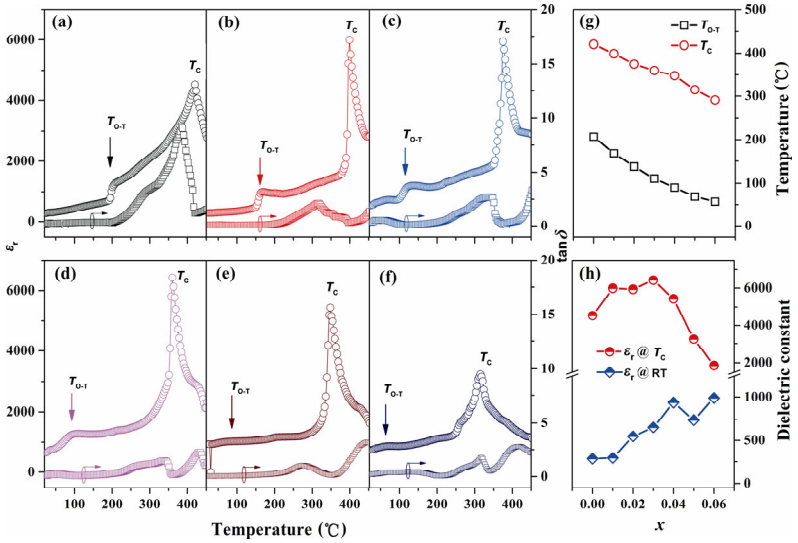

Fig. 5 Temperature dependence of dielectric constant (ε_r), $T_{O\text{-}T}$, T_C, and dielectric constant at room temperature and T_C of KNN–*x*BLZ ceramics: (a) $x = 0$, (b) $x = 0.01$, (c) $x = 0.02$, (d) $x = 0.03$, (e) $x = 0.04$, (f) $x = 0.05$, (g) $T_{O\text{-}T}$ and T_C; (h) dielectric constants at room temperature and T_C.

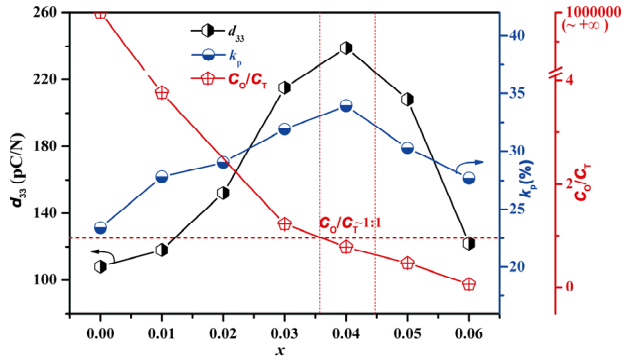

Fig. 6 Piezoelectric coefficient (d_{33}), electromechanical coupling factor (k_p), and C_O / C_T of KNN–*x*BLZ ceramics.

properties for KNN–*x*BLZ ceramics achieved at $x = 0.04$ are due to the appropriate C_O / C_T ratio (~1:1), which provides an effective method to understand the relevance between structure and performance.

Figure 7 shows the polarization electric field (*P*–*E*) hysteresis loops of KNN–*x*BLZ ceramics and remanent polarization P_r and coercive field E_c. The varying trend of remanent polarization P_r with BLZ content is similar to those of d_{33} and k_p. The peak value of remanent polarization P_r is 25.2 μC/cm^2 with $x = 0.04$. While the peak value of coercive field E_c is 1.84 kV/cm with $x = 0.05$ as shown in Fig. 7(b). For the samples with $x = 0$, 0.01, 0.02, 0.03, 0.04, 0.05, and 0.06, the corresponding remanent polarization P_r values are 7.2, 17.4, 19.3, 20.3, 25.2, 19.8, and 13.9 μC/cm^2, with coercive fields E_c of 0.88, 1.02, 1.36, 1.50, 1.52, 1.84, and 1.51 kV/cm, respectively. The peak value P_r of the sample with $x = 0.04$ is consistent with the piezoelectric property. The increase of E_c is attributed to that the increased oxygen vacancies pin the domain wall motion [37]. When KNN–*x*BLZ ceramics are doped with a large amount of BLZ ($x \geqslant 0.04$), the incorporation of Zr^{4+} would enter *B*-site and act as acceptor, which results in increased oxygen vacancies from the viewpoint of the charge neutrality. The oxygen vacancies will pin domain wall motion leading to a higher E_c. It is well known that the oxygen vacancies make the leakage current increase [38,39]. Here the gap of *P*–*E* loops is enlarged due to the raising of leakage current caused by oxygen vacancies especially when $x \geqslant 0.04$.

4 Conclusions

$Bi_{0.5}Li_{0.5}ZrO_3$ (BLZ) doped $K_{0.48}Na_{0.56}NbO_3$ (KNN) lead-free ceramics with excessive Na content were prepared to obtain high T_C and piezoelectric properties. The BLZ contents affect phase structure, microstructure, and electrical properties of KNN ceramics. All samples with adding a little BLZ exhibit O–T two-phase coexistence. Due to the appropriate proportion of O phase to T phase (C_O / C_T = 45:55), high piezoelectric properties d_{33} = 239 pC/N, k_p = 34%, and P_r = 25.23 μC/cm^2 were achieved at x = 0.04. Moreover, a high T_C = 348 ℃ was also achieved in KNN–*x*BLZ ceramics at x = 0.04. The results prove that the KNN–*x*BLZ system has promising prospects in high-temperature piezoelectric devices.

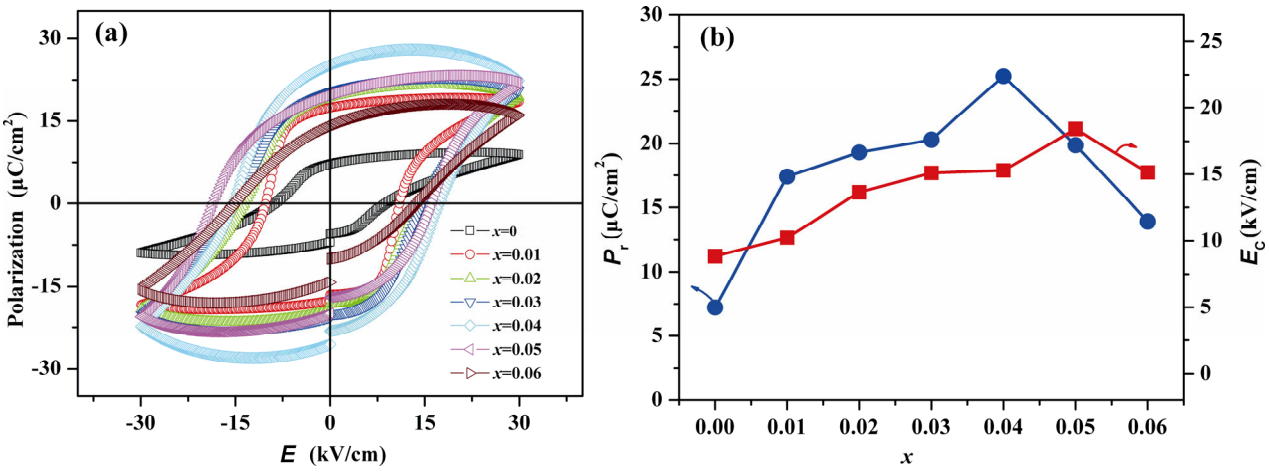

Fig. 7 *P*–*E* hysteresis loops, P_r, and E_c of KNN–*x*BLZ ceramics: (a) *P*–*E* hysteresis loops; (b) remanent polarization P_r and coercive field E_c.

Acknowledgements

This work was supported by Specialized Research Fund for the Doctoral Program of Higher Education (Grant No. 20130006110006) and National Natural Science Foundation of China (Grant Nos. 51272023 and 51472026).

References

[1] Jaffe B, Cook WR, Jaffe H. *Piezoelectric Ceramics*. Academic Press, 1971.

[2] Cross E. Materials science: Lead-free at last. *Nature* 2004, **432**: 24–25.

[3] Rödel J, Jo W, Seifert KTP, *et al*. Perspective on the development of lead-free piezoceramics. *J Am Ceram Soc* 2009, **92**: 1153–1177.

[4] Li JF, Wang K, Zhu FY, *et al*. (K,Na)NbO_3-based lead-free piezoceramics: Fundamental aspects, processing technologies, and remaining challenges. *J Am Ceram Soc* 2013, **96**: 3677–3696.

[5] Saito Y, Takao H, Tani T, *et al*. Lead-free piezoceramics. *Nature* 2004, **432**: 84–87

[6] Zheng T, Wu H, Yuan Y, *et al*. The structural origin of enhanced piezoelectric performance and stability in lead free ceramics. *Energy Environ Sci* 2017, **10**: 528–537.

[7] Xu K, Li J, Lv X, *et al*. Superior piezoelectric properties in potassium–sodium niobate lead-free ceramics. *Adv Mater* 2016, **28**: 8519–8523.

[8] Wang K, Sheng Z-Y, Zhang B-P, *et al*. (K,Na)NbO_3-based lead-free piezoceramics: Status, prospects and challenges. *J Inorg Mater* 2014, **29**: 13–22.

[9] Egerton L, Dillon DM. Piezoelectric and dielectric properties of ceramics in the system potassium–sodium niobate. *J Am Ceram Soc* 1959, **42**: 438–442.

[10] Zhang B-P, Zhang L-M, Li J-F, *et al*. Effect of sintering temperature on electrical properties of $Na_{0.5}K_{0.5}NbO_3$ lead-free piezoelectric ceramics prepared by normal sintering. *Ferroelectrics* 2007, **358**: 188–195.

[11] Wu L, Zhang JL, Wang CL, *et al*. Influence of compositional ratio K/Na on physical properties in $(K_xNa_{1-x})NbO_3$ ceramics. *J Appl Phys* 2008, **103**: 084116.

[12] Li HT, Zhang BP, Shang PP, *et al*. Phase transition and high piezoelectric properties of $Li_{0.058}(Na_{0.52+x}K_{0.48})_{0.942}NbO_3$ lead-free ceramics. *J Am Ceram Soc* 2011, **94**: 628–632.

[13] Li H, Zhang B, Li Q, *et al*. Phase and electrical properties of $[Li_{0.065}(Na_{0.535}K_{0.48})_{0.95}]NbO_3$ lead-free piezoelectric ceramics sintered at low temperature. *Adv Mater Res* 2011, **415**–**417**: 1679–1682.

[14] Wu J, Xiao D, Zhu J. Potassium–sodium niobate lead-free piezoelectric materials: Past, present, and future of phase boundaries. *Chem Rev* 2015, **115**: 2559–2595.

[15] Zheng T, Wu J, Cheng X, *et al*. New potassium–sodium niobate material system: A giant-d_{33} and high-T_C lead-free piezoelectric. *Dalton Trans* 2014, **43**: 11759–11766.

[16] Jiang L, Xing J, Tan Z, *et al*. High piezoelectricity in (K,Na)$(Nb,Sb)O_3$–(Bi,La,Na,Li)ZrO_3 lead-free ceramics. *J Mater Sci* 2016, **51**: 4963–4972.

[17] Yuan Y, Wu J, Tao H, *et al*. Composition design and electrical properties in $(1-y)(K_{0.40}Na_{0.60})_{0.985}Li_{0.015}(Nb_{1-x}Sb_x)O_3$–$yBi_{0.5}Na_{0.5}ZrO_3$ lead-free ceramics. *J Appl Phys* 2015, **117**: 084103.

[18] Shi H, Chen J, Wang R, *et al*. Full set of material constants of $(Na_{0.5}K_{0.5})NbO_3$–$BaZrO_3$–$(Bi_{0.5}Li_{0.5})TiO_3$ lead-free piezoelectric ceramics at the morphotropic phase boundary. *J Alloys Compd* 2016, **655**: 290–295.

[19] Zheng T, Wu J, Xiao D, *et al*. Potassium–sodium niobate lead-free ceramics: Modified strain as well as piezoelectricity. *J Mater Chem A* 2015, **3**: 1868–1874.

[20] Wang R, Wang K, Yao F, *et al*. Temperature stability of lead-free niobate piezoceramics with engineered morphotropic phase boundary. *J Am Ceram Soc* 2015, **98**: 2177–2182.

[21] Cheng X, Wu J, Zheng T, *et al*. Rhombohedral–tetragonal phase coexistence and piezoelectric properties based on potassium–sodium niobate ternary system. *J Alloys Compd* 2014, **610**: 86–91.

[22] Cheng X, Wu J, Lou X, *et al*. Achieving both giant d_{33} and high T_C in patassium–sodium niobate ternary system. *ACS Appl Mater Interfaces* 2014, **6**: 750–756.

[23] Zhang B, Wu J, Wang X, *et al*. Rhombohedral–orthorhombic phase coexistence and electrical properties of Ta and $BaZrO_3$ co-modified (K,Na)NbO_3 lead-free ceramics. *Curr Appl Phys* 2013, **13**: 1647–1650.

[24] Zushi J, Ariizumi T, Kojima S, *et al*. Formation of morphotropic phase boundary in $(Na_{0.5}K_{0.5})NbO_3$–$BaZrO_3$–$(Bi_{0.5}Li_{0.5})TiO_3$ lead-free piezoelectric ceramics. *Jpn J Appl Phys* 2013, **52**: 07HB02.

[25] Cheng X, Wu J, Wang X, *et al*. Giant d_{33} in (K,Na)$(Nb,Sb)O_3$–(Bi,Na,K,Li)ZrO_3 based lead-free piezoelectrics with high T_C. *Appl Phys Lett* 2013, **103**: 052906.

[26] Zhang B, Wu J, Cheng X, *et al*. Lead-free piezoelectrics based on potassium–sodium niobate with giant d_{33}. *ACS Appl Mater Interfaces* 2013, **5**: 7718–7725.

[27] Liang W, Wu W, Xiao D, *et al*. Construction of new morphotropic phase boundary in $0.94(K_{0.4-x}Na_{0.6}Ba_xNb_{1-x}Zr_x)O_3$–$0.06LiSbO_3$ lead-free piezoelectric ceramics. *J Mater Sci* 2011, **46**: 6871–6876.

[28] Zhen Y, Li JF. Normal sintering of (K,Na)NbO_3-based ceramics: Influence of sintering temperature on densification, microstructure, and electrical properties. *J Am Ceram Soc* 2006, **89**: 3669–3675.

[29] Park S-H, Ahn C-W, Nahm S, *et al*. Microstructure and piezoelectric properties of ZnO-added $(Na_{0.5}K_{0.5})NbO_3$ ceramics. *Jpn J Appl Phys* 2004, **43**: L1072–L1074.

[30] Kim MS, Jeong SJ, Song JS. Microstructures and piezoelectric properties in the Li_2O-excess $0.95(Na_{0.5}K_{0.5})NbO_3$–$0.05LiTaO_3$ ceramics. *J Am Ceram Soc* 2007, **90**: 3338–3340.

[31] Mgbemere HE, Hinterstein M, Schneider GA. Structural

phase transitions and electrical properties of $(K_xNa_{1-x})NbO_3$-based ceramics modified with Mn. *J Eur Ceram Soc* 2012, **32**: 4341–4352.

[32] Wu J, Xiao J, Zheng T, *et al*. Giant piezoelectricity of $(K,Na)(Nb,Sb)O_3$–$(Bi,Na,K,Pb)ZrO_3$ ceramics with rhombohedral–tetragonal (R–T) phase boundary. *Scripta Mater* 2014, **88**: 41–44.

[33] Zhou J-J, Cheng L-Q, Wang K, *et al*. The phase structure and electric properties of low-temperature sintered $(K,Na)NbO_3$-based piezoceramics modified by CuO. *Ceram Int* 2014, **40**: 2927–2931.

[34] Paula AJ, Parra R, Zaghete MA, *et al*. Study on the $K_3Li_2Nb_5O_{15}$ formation during the production of $(Na_{0.5}K_{0.5})_{(1-x)}Li_xNbO_3$ lead-free piezoceramics at the morphotropic phase boundary. *Solid State Commun* 2009, **149**: 1587–1590.

[35] Dai Y, Zhang X, Zhou G. Phase transitional behavior in $K_{0.5}Na_{0.5}NbO_3$–$LiTaO_3$ ceramics. *Appl Phys Lett* 2007, **90**: 262903.

[36] Zuo R, Fu J, Lv D. Phase transformation and tunable piezoelectric properties of lead-free $(Na_{0.52}K_{0.48-x}Li_x)(Nb_{1-x-y}Sb_yTa_x)O_3$ system. *J Am Ceram Soc* 2009, **92**: 283–285.

[37] Li E, Kakemoto H, Wada S, *et al*. Influence of CuO on the structure and piezoelectric properties of the alkaline niobate-based lead-free ceramics. *J Am Ceram Soc* 2007, **90**: 1787–1791.

[38] Singh SK, Maruyama K, Ishiwara H. Reduced leakage current in La and Ni codoped $BiFeO_3$ thin films. *Appl Phys Lett* 2007, **91**: 112913.

[39] Yin LH, Zhao BC, Fang J, *et al*. Improved leakage current and ferromagnetic properties in magnetic field annealed $BiFeO_3$-based ceramics. *J Solid State Chem* 2012, **194**: 194–198.